Wang *et al.*
European Journal of Medical Research (2025) 30:408
https://doi.org/10.1186/s40001-025-02642-z

European Journal of Medical Research

RESEARCH

Open Access

Identification of shared mechanisms between Alzheimer's disease and atherosclerosis by integrated bioinformatics analysis

Jukun Wang[1,3], Jing Yao[2*] and Zhe Wang[1,3*]

Abstract

Alzheimer's disease (AD) and atherosclerosis (AS) are two interacting diseases mostly affecting aged adults. AD is characterized by the deposition of neuritic plaques mainly consisting of Aβ, and AS is defined by the formation of atheromatous plaque along the vascular wall. The shared mechanisms underlying the pathogenesis of AD and AS remain unclear. Here we applied several bioinformatic analyses of bulk sequencing data sets of AD brain tissues and atherosclerotic plaques to seek relevant genes between AD and AS. *WIPF3*, was identified as the most affected gene in both diseases using weighted gene co-expression network analysis, machine-learning-based Lasso Cox regression analysis and random forest analysis. Furthermore, immune cell infiltration analysis of AS data sets and cell portion of single-cell RNA sequencing data from AD patients revealed an essential role of inflammation in the co-occurrence of AD and AS. Taken together, *WIPF3* deficiency and inflammation may simultaneously mediate both AD and AS and could be potential targets for the prevention and therapy of these two closely related diseases.

Keywords Alzheimer's disease, Atherosclerosis, WGCNA, Machine learning, WIPF3

Introduction

Alzheimer's disease (AD) is a progressive and irreversible neurodegenerative disorder the most prevalent subtype of dementia. It is characterized by amyloid-β (Aβ) deposition (also known as neuritic plaques) and intraneuronal aggregates of hyperphosphorylated tau (neurofibrillary tangles). Approximately 10% of individuals over the age of 65 are affected by Alzheimer's disease (AD), and currently, there are limited options available to effectively manage or improve symptoms [1, 2]. The cause of AD is still unknown. Ageing, type-II diabetes, brain trauma, and cardiovascular diseases including AS are the major risks of AD. A growing amount of evidence suggests that vascular aging accompanies or even precedes the development of AD pathology [3, 4].

Vascular aging, referring to the age-related vascular changes, critically influences the structural and functional integrity of the brain. The neurovascular unit, a notion formally raised in 2001, emphasizes the relationship between neuronal cells and blood vessels, and has attracted the attention to the interdependence between neurodegenerative diseases and vascular diseases [4]. Vascular aging inside and outside the central

*Correspondence:
Jing Yao
jingyao9420@163.com
Zhe Wang
wangz@xwhosp.org
[1] Department of General Surgery, Xuanwu Hospital, Capital Medical University, Beijing, China
[2] Cerebrovascular Disease Department, Neurological Disease Center, Beijing Anzhen Hospital, Capital Medical University, Beijing, China
[3] The National Clinical Research Center for Geriatric Disease, Xuanwu Hospital, Capital Medical University, Beijing, China

nervous system are both more severe in AD. The prevalence of vascular pathology, including microinfarcts, lacunes, and moderate to severe atherosclerosis (AS), especially AS in the circle of Willis, is higher in AD patients than in patients with α-synucleinopathy or frontotemporal lobar degeneration [5–7]. Clinical studies also suggested that the incidence of AD increases in participants with severe carotid and femoral AS [8]. A recent study demonstrated that the widespread sensory and sympathetic nerve fibres arising near immune cells and media smooth muscle cells (SMCs) in plaque-laden regions and suggested that atheromatous plaque can induce the sympathetic nerve activation in the brain, which, in turn, promotes atheromatous plaque growth via increasing sympathetic projections to the artery [9].

AS, can be augmented by vascular aging, is the major cause of mortality worldwide [10, 11]. The hallmarks of AS are the trans-differentiation of vascular SMC (vSMC) occurring beneath the endothelial cells and the fibrous plaque formation, induced by the lipid deposition and calcification, in the subendothelial space of arterial. The trans-differentiated vSMC, together with the immune cells recruited to lesion from the circulation, promote immune responses. AS in the central nervous system and the periphery may cut or reduce the supply of oxygen and energy to the brain, leading to hypoxia, neuroinflammation, and neuronal death, which facilitates AD pathogenesis.

An increasing body of evidence suggests a significant overlap between AD and AS etiologies, and their mutually correlated onset and progression [12, 13]. AD and AS share common risk factors, including aging, sex, and risk genes [14–19]. Therein, the presence of ApoE ε4 allele substantially increases the risks of both AD and AS, suggesting shared molecular mechanisms underlying these two diseases. Therefore, identifying molecular pathways and genes involved in both AD and AS will facilitate the elucidation of their pathogenesis and the development of preventative or therapeutic methods.

In this study, we sought to find common pathways and genes involved in the pathogenesis of AD and AS based on the public databases through various bioinformatics techniques. The result suggested that the under expression of gene *WIPF3* was correlated with both of the two diseases, and this conclusion was confirmed with a validation data set. Moreover, we evaluate the role of inflammation in AD and AS via immune cell infiltration and cell portion analysis. These findings added new insight into the shared cellular and molecular mechanism in the etiologies of AD and AS, and may facilitate the development of novel therapeutic strategies.

Methods

Data collection and processing

In this study, we utilized the GEOquery package in R software to download four data sets from the Gene Expression Omnibus (GEO) database (https://www.ncbi.nlm.nih.gov/geo/), including GSE36980, GSE173955, GSE43292, and GSE1009275. Among these, GSE36980 and GSE173955 were used to for AD, GSE43292 and GSE100927 were used for AS. Before starting the analyses, we normalized the gene expression data to remove batch effects.

The GSE36980 data set (the training data set) comprises a total of 80 samples, with 8 samples derived from the hippocampal region of brain tissues of AD patient donors, and 10 samples derived from the hippocampal region of brain tissues from non-AD patient donors. The gene expression data was collected using the Affymetrix Human Gene 1.0 ST platform. The GSE173955 data set ($n=18$) was chosen for external validation, including 8 samples from the hippocampal region of brain tissues from elderly patients with AD and 10 samples from the hippocampal region of brain tissues from non-elderly patients without AD. This data set was generated using the Illumina TruSeq stranded mRNA LT Sample Prep kit for library preparation and sequenced on the HiSeq1500 platform to obtain the transcriptomic data. The GSE43292 (training data set) data set contains 64 samples, including 32 carotid atheroma plaque and 32 normal tissue adjacent to carotid artery plaques. The gene expression data was generated with the Affymetrix Human Gene 1.0 ST array. GSE100927 contains 104 samples, of which 26 atherosclerotic femoral artery tissues and 12 control femoral artery tissues were used for validation. The gene expression data for this data set was generated using the Agilent SurePrint G3 Human GE v2 8×60K Microarray platform.

Single-cell RNA sequencing data set of AD were also obtained from the GEO database (GSE175814) containing 2 of AD and 2 age- and gender-matched control post-mortem brain samples (anterior hippocampal cortex) [20]. All the samples were re-analyzed for result validation.

The single-cell data analysis was performed based on the raw UMI counts data. Seurat v4.3 was utilized in the data preprocessing, including quality control, normalization, as well as dimensionality reduction clustering [21]. To identify the inter-sample anchors for integration, we utilized the FindIntegrationAnchors function of the Seurat to identify the top 2000 consistently and highly variable genes among the samples. Then, we employed the IntegrateData function to acquire a combined and centered expression matrix. Subsequently, data normalization and identification of highly variable genes were

performed. We retained barcodes with expression of at least 500 genes and no more than 4000 total genes, as well as no more than 15% mitochondrial genes. The NormalizeData and FindVariableFeatures functions were used to normalize the expression matrix and calculate highly variable genes. Subsequently, the ScaleData function was utilized to standardize the expression matrix.

Cell clustering and cell type determination of single-cell RNA sequencing data

Principal component analysis (PCA) was conducted on the preprocessed expression matrix. We utilized the top 16 principal components to build the shared nearest neighbor (SNN) cell graph, and the FindClusters function was then applied to cluster the graph with a resolution of 0.5. The Uniform Manifold Approximation and Projection (UMAP) algorithm was utilized to embed the top 16 principal components onto two dimensions [22]. Marker genes for each cluster were calculated using the FindAllMarkers function based on the Wilcoxon test, with the criteria of p value < 0.05. The processed expression matrix was then subjected to subsequent analysis to identify cell populations.

Clusters were annotated manually. Based on the CellMarker database (http://bio-bigdata.hrbmu.edu.cn/CellMarker/) and the previous studies, the specific cell types were annotated by the expression of canonical markers: inhibitor neurons (*GAD1, GAD2*), excitatory neurons (*SLC17A7*), microglia (*TYROBP, CX3CR1*), astrocytes (*AQP4*), oligodendrocyte precursor cells (*PDGFRA, MYT1*), fibroblasts (*COL1A2*), oligodendrocytes (*OPALIN*), endothelial cells (*NOSTRIN, CLDN5*), pericytes (*KCNJ8*), and peripheral blood mononuclear cells (*CD3E*) for the GSE175814 data sets.

Differential expression analysis of GSE36980 and GSE43292

For RNA-seq data in GSE36980 and GSE43292, we used limma package in R software to identify differentially expressed genes (DEGs) between diseased and normal samples. A p value < 0.05 and |log2 (FC)| value > 0 was considered significant.

Weighted gene co-expression network analysis

To further understand the role of genes in the development of AD and AS, we performed weighted gene co-expression network analysis (WGCNA) with the R package WGCNA in R software. WGCNA can be used to identify co-expressed genes modules whose expression plays a facilitating or inheriting role in the development of disease, and the correlation of modules with disease characterization was calculated. Before starting the analysis, the hclust function of the WGCNA package was used to cluster samples and remove obvious outliers. The pickSoftThreshold function in the WGCNA package was performed to determine the optimal soft threshold and adjacencies. Then, the adjacency matrix was transformed into a topological overlap matrix (TOM). Furthermore, based on a minimum module size of 30 genes, dynamic tree cut algorithm was used to identify co-expression gene modules. We then calculated the relationship between the gene modules and disease characteristics via gene significance (GS) and module membership (MM) and ultimately identified the key modules [23].

Enrichment analyses of both DEGs and genes in the key modules

The biological processes, cellular components, and molecular functions of both DEGs and the genes in the key modules were determined using Gene Ontology (GO) analysis. The pathways of both DEGs and the genes in the key modules were explored using Kyoto Encyclopedia of Genes Genomes (KEGG) and Gene Set Enrichment Analysis (GSEA). We used the clusterProfiler package in R software to investigate and visualize the enrichment analyses. The false discovery rate (FDR) < 0.05 were considered significantly enriched.

Identification and validation of potential shared diagnostic biomarkers in AD and AS

To further narrow down the range of potential candidate genes, the UpSetR packages in R software was used to visualize the intersection of DEGs obtained from the GSE data sets and key gene modules identified by WGCNA. Least absolute shrinkage and selection operator (Lasso) Cox regression analysis and random forest analysis were used to further screen the core markers from above intersection of DEGs and modules gene. Boxplot was utilized to reveal the relationship between the core gene expression levels and disease characteristics in the training and validation data sets. Receiver operating characteristic (ROC) curves were used to evaluate and validate the pathogenic value of core gene.

Cell culture and treatment

Mouse vascular smooth muscle cell line MOVAS-1 was purchased from American Tissue Culture Collection (ATCC) and was cultured in DMEM with 10% fetal bovine serum. Cells were maintained at 37 °C (5% CO_2). 2 μM Aβ were added to the wells of 6-well plates.

Real-time PCR

Total RNA was extracted from MOVAS-1 using the FastPure Cell/Tissue Total RNA Isolation Kit V2 (RC112, Vazyme, Nanjing, China). The complementary DNA template was transcribed using HiScript III 1st Strand cDNA

Synthesis Kit (RC312, Vazyme, Nanjing, China). Real-time (RT)-PCR was performed using ChamQ SYBR qPCR Master Mix (Q311, Vazyme, Nanjing, China) in a LightCycler 480, and the data was analyzed using LightCycler 480 Software. The relative mRNA expression of the target gene was determined according to the formula of $2-\Delta\Delta Ct$. Primers for qPCR were presented as following: WIPF3 forward: 5′-CACGTTCCACTCCATGGAAGAC-3′, reverse: 5′-GAGTACAGTAGAGTCTCGAGG-3′; GAPDH forward: 5′-AGGTCATCCCAGAGCTGAACG-3′; reverse: 5′-CACCCTGTTGCTGTAGCCGTAT-3′.

Immune cell infiltration analysis

R package IOBR [24] was used to confirm the relationship between the infiltration levels of various immune cells and disease characteristics in GSE36980 and GSE43292, respectively. 22 types of immune cells are included in this infiltration analysis: naïve B cells, memory B cells, plasma cells, CD8+T cells, naïve CD4+T cells, resting memory CD4+T cells, activated memory CD4+T cells, T follicular helper cells (Tfhs), regulatory T cells (Tregs), and gamma delta T (Tgd) cells, resting natural killer (NK) cells, activated NK cells, monocytes, macrophages (M0–M2), resting dendritic cells, activated dendritic cells, resting mast cells, activated mast cells, eosinophils, and neutrophils. All statistical p values were two-sided, and for single-cell and bulk RNA-seq differential gene selection, a p value < 0.05 or an adj. p value < 0.05 was considered statistically significant. For other statistical tests, the p value or adj. p value criteria were as described in the text.

Statistical analysis

In the study, all statistical analyses were performed using R software (version 4.2.3). Wilcoxon test was used to compare the differences in the gene expression and levels of immune cell infiltration between two groups, whereas one-way analysis of variance (ANOVA) was used to test the differences among the three groups. The correlation analyses were performed using Spearman's correlation analysis. Lasso Cox regression analysis and random forest were used to identify core gene. The area under the ROC curve (AUC) was also employed to assess the diagnostic efficiency of core gene. All statistical p values were two-sided, and a p value < 0.05 or an adj. p value < 0.05 was considered statistically significant. Single, double, triple asterisks refer to 0.05, 0.01, 0.001 level, respectively.

Results

Identification and functional enrichment of DEGs both in the GSE36980 and GSE43292

The flow diagram of this study is shown in Fig. 1. To investigate whether shared mechanisms exist or not between AD and AS, we first applied differential expression analysis on AD data set GSE36980 and AS data set GSE43292. According to the thresholds mentioned in the methods section, there were a total of 4149 DEGs in the GSE36980, including 1164 up-regulated genes and 2985 down-regulated genes. In GSE43292 data set, 7597DEGs were obtained, of which 3456 genes were up-regulated and 4141 genes were down-regulated. The heatmap and volcano plots of DEGs in two data sets are shown in Fig. 2A–D.

Functional enrichment analyses were also conducted on the DEGs of both data sets. For GSE36980, GO enrichment analysis showed that DEGs were involved in biological processes, such as the modulation of chemical synaptic transmission, the regulation of trans-synaptic signaling, the vesicle-mediated transport in synapse, neurotransmitter transport and synaptic vesicle cycle (Fig. 3A). As shown in the KEGG analysis, DEGs were enriched in neurodegeneration, Synaptic vesicle cycle and Alzheimer disease (Fig. 3B). GSEA results suggested that DEGs were involved in synaptic signaling, synaptic vesicle exocytosis, and postsynaptic specialization membrane (Fig. 3C). GO enrichment analysis revealed that DEGs in the GSE43292 were associated with biological process, such as positive regulation of cell adhesion, myeloid leukocyte activation, regulation of T cell activation and mononuclear cell differentiation (Fig. 3D). KEGG enrichment analysis showed that these DEGs were enriched in pathways, such as regulation of actin cytoskeleton and chemokine signaling pathway (Fig. 3E). GSEA results indicated that immune response plays a role in the development of atherosclerosis (Fig. 3F).

WGCNA and functional enrichment of module gene

To identify key modules in both AD and AS, we further conducted WGCNA on data sets GSE36980 and GSE43292. WGCNA was performed to identify module of genes with altered expressions associated with these two diseases, and the key module was selected according to the correlation of gene modules with diseases. We used the Pearson's correlation coefficient to cluster the samples in the GSE36980 and GSE43292. After removing outliers, sample clustering trees of both GSE36980 and GSE43292 are plotted in Fig. 4A, B. A soft threshold power of $\beta=6$ was determined for the AD model, and the soft threshold power in the AS modeling was set as 12 (Fig. 4C, D). After merging similar gene modules, 18 modules were identified in the AD model set (Fig. 4E) and 22 modules in the AS model set (Fig. 4F). We calculated the correlation between each module and disease characteristics. The correlations between the disease severity and the modules are shown in Fig. 4E, F. The darkturquoise module showed maximum positive association with AD occurrence ($r=0.54$, $p=0.03$), and the

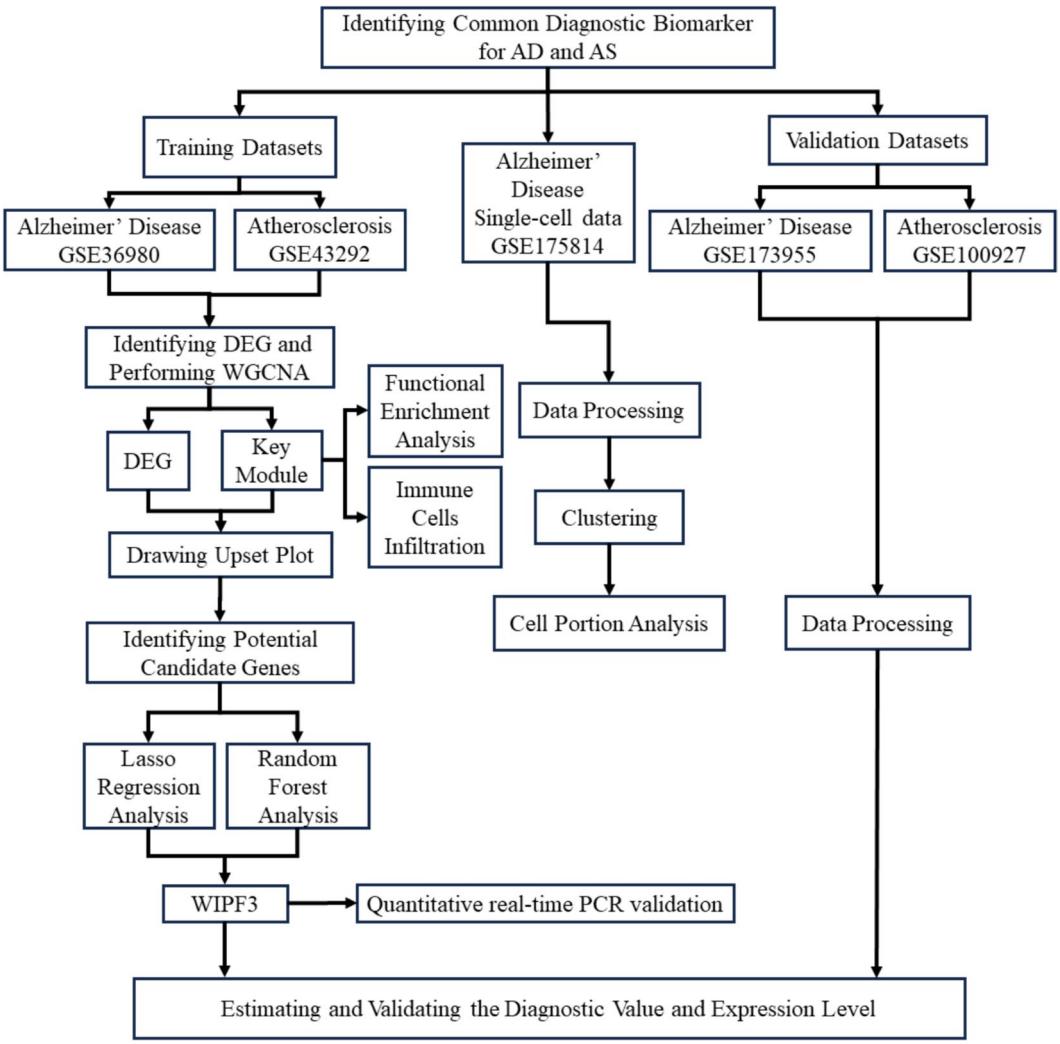

Fig. 1 Flow chart showing the scheme of this study

brown4 module had maximum negative association with AD occurrence ($r=-0.73$, $p=0.001$) (Fig. 4E). In the AS modeling set, the black module had the greatest positive correlation with the occurrence of AS ($r=0.59$, $p=3e-7$) and the brown module had the greatest negative correlation with the occurrence of AS ($r=-0.52$, $p=1e-05$) (Fig. 4F).

In addition, genes included in individual modules were assessed for functional enrichment according to GO and KEGG. Functional and pathways enrichment of the darkturquoise module genes were mainly annotated to keratinocyte differentiation, skin development, epidermal cell differentiation, protein digestion and absorption, linoleic acid metabolism, cytokine–cytokine receptor interaction, primary immunodeficiency, and vascular smooth muscle contraction. The brown4 module genes were mainly involved in cellular respiration, aerobic respiration, ATP metabolic process, ATP synthesis coupled electron transport, neurodegeneration, ubiquinone and other terpenoid–quinone biosynthesis and Alzheimer disease (Supplemental Fig. 1). The black module genes were mainly involved in positive regulation of cytokine production, negative regulation of immune system, immune response, regulation of T cell activity, leukocyte proliferation, cell receptor signaling pathway, T cell receptor signaling pathway, Th17 cell differentiation, chemokine signaling pathway as well as Th1 and Th2 cell differentiation.

The brown module genes were mainly associated with the regulation of cell-matrix adhesion, negative regulation of cell junction, the regulation of cell-substrate adhesion, actin filament-based movement, cell junction assembly, the regulation of focal adhesion assembly, the regulation of cell-substrate junction assembly, TGF-beta signaling pathway, Wnt signaling pathway,

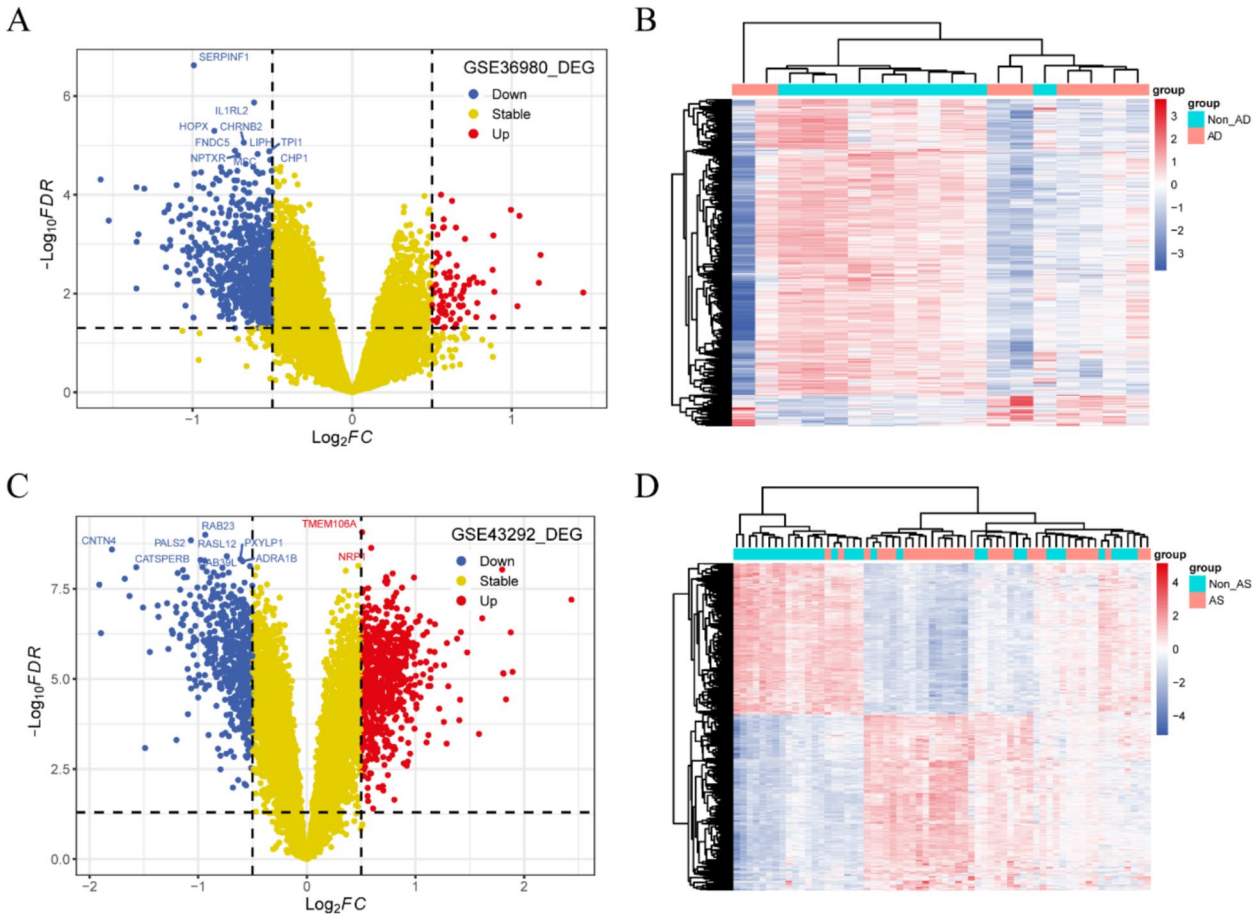

Fig. 2 Identification of DEGs in the GSE36980 and GSE43292. **A** Volcano plots of DEGs in the GSE36980. **B** Heatmap plots of DEGs in the GSE36980. **C** Volcano plots of DEGs in the GSE43292. **D** Heatmap plots of DEGs in the GSE43292

p53 signaling pathway and cytokine–cytokine receptor interaction (Supplemental Fig. 2).

WIPF3 was identified as a common pathogenic molecular for AD and AS

As shown in Fig. 5A, a total of 123 genes were potentially associated with both of AD and AS, including 112 positively correlated genes and 11 negatively correlated genes. To further identify core pathogenic molecular, these 123 genes were subjected to the Lasso Cox regression and random forest analysis (Fig. 5B–E). In the 123 genes, three including *TTPAL, WIPF3,* and *EGFLAM* were identified in GSE36980 as being possibly pathogenic, and five (*WIPF3, RIMS1, C8orf48, HSPA4,* and *DOK6*) were identified in GSE43292 to be possibly pathogenic (Table 1). Finally, we confirmed that the altered expression of *WIPF3* was common for the pathogenesis of both AS and AD.

Furthermore, we performed ROC analysis to estimate the pathogenic efficiency of WIPF3 for AD and AS. In GSE36980, and the result showed that the AUC was 0.900 (Fig. 6A) and in GSE43292, AUC was 0.796 (Fig. 6A). GSE173955 and GSE100927, as two external data sets obtained from GEO database, were used to verify the relationship between AD or AS identification and mRNA levels of *WIPF3*. We found that the AUC was 0.899 based on GSE173955 (Fig. 6B). In GSE100927, the AUC was 0.889 (Fig. 6B). In addition, we plotted Boxplot to investigate the relationship between WIPF3 expression and disease characteristics in AD and AS. The expression of *WIPF3* was significantly down-regulated in samples of AD and AS based on the training and validation data sets (Fig. 6C, D). To further confirm the role of WIPF3 in AD and AS, we treated the MOVAS-1 with Aβ overnight and detected their mRNA level of *WIPF3* using RT-PCR. Results in Fig. 6E showed that WIPF3 was significantly down-regulated in Aβ-treated MOVAS-1 as compared with the untreated cells ($p < 0.05$). These results indicate that *WIPF3* may potentially play a role in the shared pathogenesis of AD and AS.

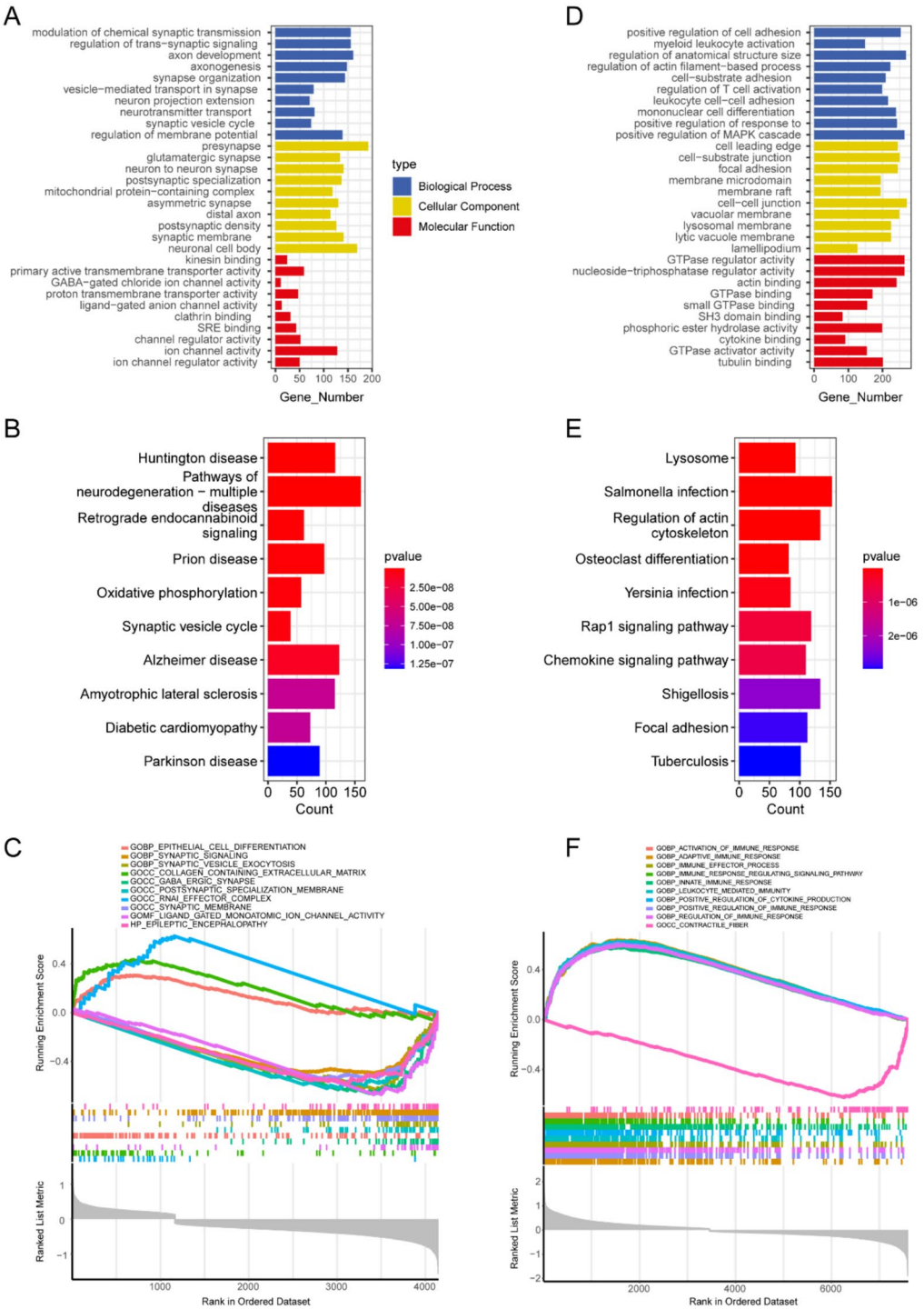

Fig. 3 Functional enrichment analysis of DEGs in the GSE36980 and GSE43292. **A** GO analysis of DEGs in the GSE36980. **B** KEGG analysis of DEGs in the GSE36980. **C** GSEA analysis of DEGs in the GSE36980. **D** GO analysis of DEGs in the GSE43292. **E** KEGG analysis of DEGs in the GSE43292. **F** GSEA analysis of DEGs in the GSE43292

Immune cell infiltration both in AD and AS

The afore-mentioned results suggest that inflammation is implicated in AS and AD. To confirm whether immunity could affect disease progression of these two diseases, we analyzed the infiltrating levels of 22 immune cell types between diseased and non-diseased

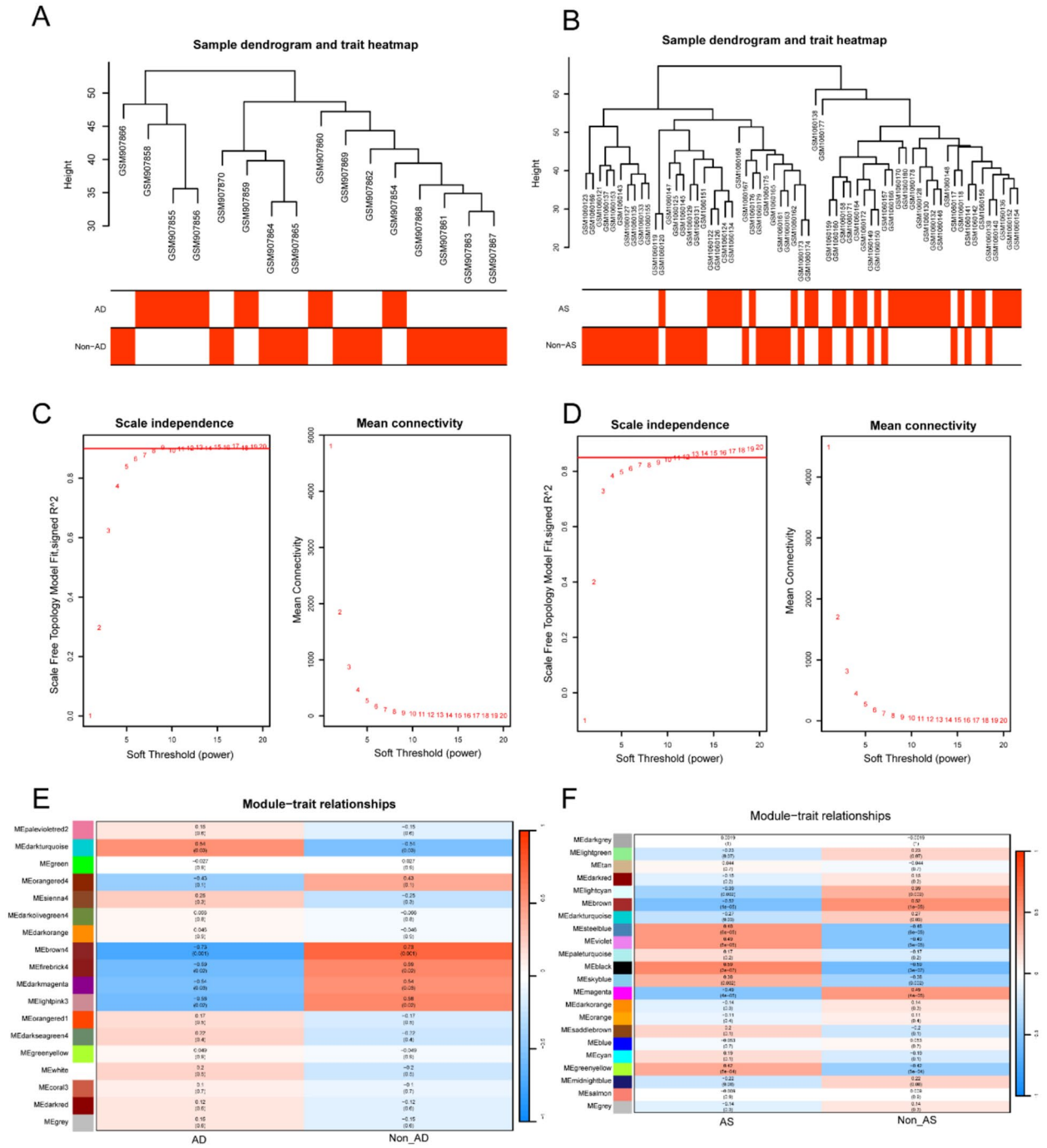

Fig. 4 WGCNA was performed for the GSE36980 and GSE43292. **A** Clustering dendrogram of 16 samples after removing outlier in the GSE36980. **B** Clustering dendrogram of 63 samples after removing outlier in the GSE43292. **C** Determination of soft-threshold power in the WGCNA for the GSE36980. **D** Determination of soft-threshold power in the WGCNA for the GSE43292. **E** Heatmap showing correlation between modules and disease characteristics for the GSE36980. **F** Heatmap showing correlation between modules and disease characteristics for the GSE43292

samples. These infiltrating immune cells types included those related to adaptive immunity, such as naïve B cells, memory B cells, plasma cells, CD8+ T cells, naïve CD4+ T cells, resting memory CD4+ T cells, activated memory CD4+ T cells, T follicular helper cells (Tfhs), regulatory T cells (Tregs), and gamma delta T (Tgd) cells, and those related to innate immunity including resting natural killer (NK) cells, activated NK cells,

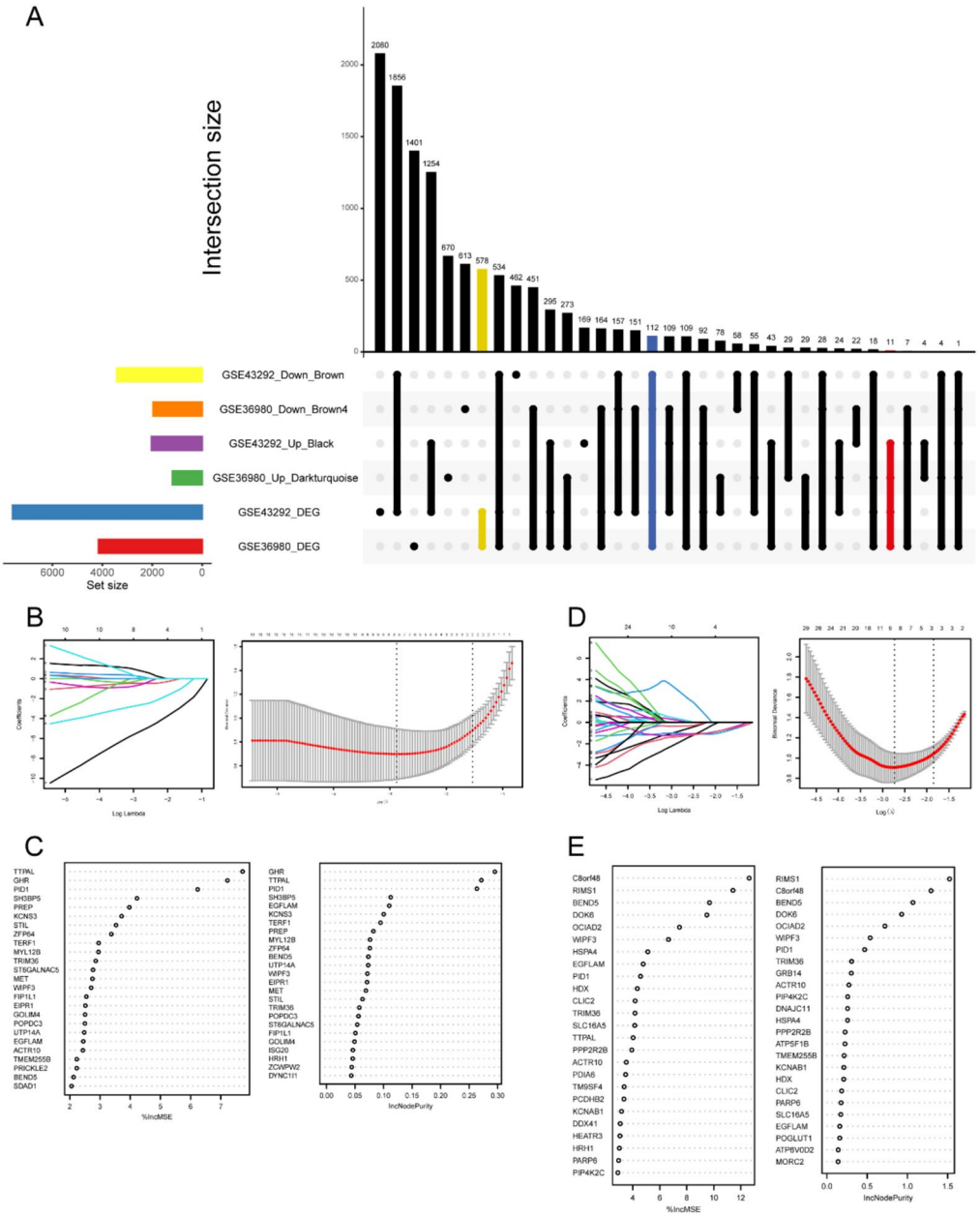

Fig. 5 Identification of core diagnostic biomarker based on intersection genes among different genes lists. **A** UpSet diagram shows that a total of 123 genes potentially involved in pathogenesis of AD and AS. **B** Lasso Cox regression analysis was conducted to screen candidate biomarkers based on 123 genes in GSE43292. **C** Random forest analysis was conducted to screen top 25 candidate biomarkers based on 123 genes in GSE43292. **D** Lasso Cox regression analysis was conducted to screen candidate biomarkers based on 123 genes in GSE36980. **E** Random forest analysis was conducted to screen top 25 candidate biomarkers based on 123 genes in GSE36980

monocytes, macrophages (M0–M2), resting dendritic cells, activated dendritic cells, resting mast cells, activated mast cells, eosinophils, and neutrophils. The infiltration portion of 22 immune cell types in samples from AD and AS training data sets are shown in Fig. 7A, B. However, we did not observe significant difference of immune cell infiltration between samples with and without AD (Fig. 7C). Whereas, for samples with and without AS, significant differences were observed in various infiltrated immune cells, such as naive B cells, memory B cells, CD8+ T cells, activated memory CD4+ T cells, regulatory T cells, activated NK cells, monocytes, M0 macrophages, activated dendritic cells and neutrophils (Fig. 7D).

Table 1 Candidate pathogenic genes associated with AD and AS identified in datasets GSE36980 and GSE43292

AD_LassoRegression	AD_%IncMSE	AD_IncNodePurity
TTPAL	TTPAL	GHR
WIPF3	GHR	TTPAL
KCNS3	PID1	PID1
GOLIM4	SH3BP5	SH3BP5
SDAD1	PREP	EGFLAM
TMEM255B	KCNS3	KCNS3
NAP1L1	STIL	TERF1
EGFLAM	ZFP64	PREP
	TERF1	MYL12B
	MYL12B	ZFP64
	TRIM36	BEND5
	ST6GALNAC5	UTP14A
	MET	WIPF3
	WIPF3	EIPR1
	FIP1L1	MET
	EIPR1	STIL
	GOLIM4	TRIM36
	POPDC3	POPDC3
	UTP14A	ST6GALNAC5
	EGFLAM	FIP1L1
	ACTR10	GOLIM4
	TMEM255B	ISG20
	PRICKLE2	HRH1
	BEND5	ZCWPW2
	SDAD1	DYNC1I1

AS_LassoRegression	AS_%IncMSE	AS_IncNodePurity
WIPF3	C8orf48	RIMS1
RIMS1	RIMS1	C8orf48
C8orf48	BEND5	BEND5
DNAJC11	DOK6	DOK6
LIPC	OCIAD2	OCIAD2
ACTR10	WIPF3	WIPF3
METTL1	HSPA4	PID1
HSPA4	EGFLAM	TRIM36
DOK6	PID1	GRB14
	HDX	ACTR10
	CLIC2	PIP4K2C
	TRIM36	DNAJC11
	SLC16A5	HSPA4
	TTPAL	PPP2R2B
	PPP2R2B	ATP5F1B
	ACTR10	TMEM255B
	PDIA6	KCNAB1
	TM9SF4	HDX
	PCDHB2	CLIC2
	KCNAB1	PARP6
	DDX41	SLC16A5
	HEATR3	EGFLAM
	HRH1	POGLUT1
	PARP6	ATP6V0D2
	PIP4K2C	MORC2

To further evaluate the effects of immune responses in AD, we applied single-cell data GSE175814 to further detect the immune cell infiltration in the brain. We performed dimensionality reduction after data processing. Subsequently, using principal component analysis and UMAP analysis, the cells were partitioned into 23 clusters (Fig. 8A). Based on canonical markers for specific cell types, cells within these 23 clusters were further classified into nine main clusters: inhibitory neurons, excitatory neurons, microglia, astrocytes, oligodendrocyte precursor cells, oligodendrocytes, endothelial cells, pericytes, and peripheral blood mononuclear cells (Fig. 8B, C). Then, we analyzed the portion of different cells in hippocampus between AD and non-AD controls. The results demonstrated that the portion of microglia and astrocytes were higher in AD patients than those in non-AD controls (Fig. 8D).

Discussion

AD and AS are two different pathological conditions but are interconnected in many aspects. They share some risk factors and overlapping pathophysiological mechanisms. Both diseases are associated with aging, APOE ε4, high cholesterol levels, high blood pressure, obesity, smoking and other risk factors [25, 26]. These factors contribute to the inflammatory response, oxidative stress, ER stress, vascular pathologies, and endothelial dysfunction which are common for both AD and AS. Studies have also suggested that cerebral AS may increase the risk of AD, and AS-induced reduction in blood flow to the brain may impair the pathological Aβ clearance, leading to Aβ accumulation, Aβ plaque formation, and subsequent neurodegeneration [27]. Nevertheless, the exact molecular mechanisms linking AD and AS are largely unknown. Hence, this study aims to uncover the shared mechanisms responsible for the development of both AD and AS.

Here, we applied several bioinformatic methods to evaluate the differences and similarities between AD and AS at the level of gene expressions. First, we compared the transcription profiles of AD and AS, the DEGs and the functional enrichment analysis suggested that the causes of AD and AS seems incompatible. To further confirm the association between AD and AS, WGCNA was performed to identify the key modules between AD and AS. Next, we employed two machine-learning algorithms, Lasso Cox regression analysis and random forest analysis, to ascertain the most significant pathogenic impact of shared genes in AD and AS. As a result, we pinpointed out one gene, WIPF3, with notable pathogenic impact. Finally, as the aforementioned analysis points to the role of inflammation in both AD and AS, we explore the immune cell infiltration of AD and AS, the results confirmed the importance of inflammatory response in both diseases.

Through WGCNA, we screened out several relevant modules in AD and AS. It is not feasible to study the roles of all genes identified in the most relevant modules,

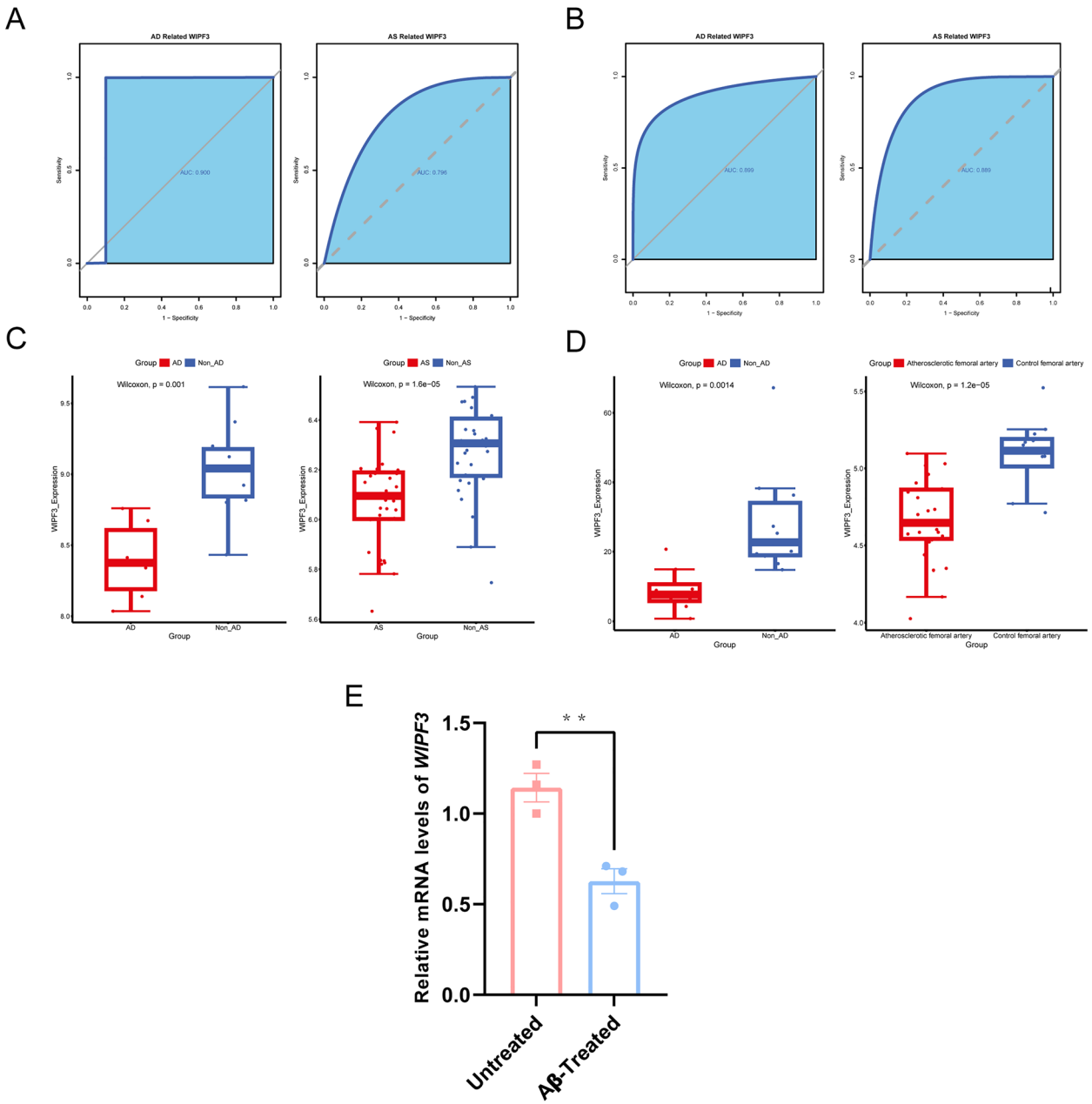

Fig. 6 Diagnostic value of WIPF3 and its differential expression between diseased and normal samples for AD and AS. **A** ROC curve evaluating the WIPF3 diagnostic value in GSE36980 and GSE43292. **B** ROC curve evaluating the WIPF3 diagnostic value in GSE173955 and GSE100927. **C** Boxplot showing the differential expression levels between diseased and normal samples in GSE36980 and GSE43292. **D** Boxplot showing the differential expression levels between diseased and normal samples in GSE173955 and GSE100927

screening out one or several most relevant gene(s) for AD and AS is necessary. Currently, machine learning has emerged as a pivotal technique for pinpointing essential genes, which are implicated in the discovery of therapeutic targets and diagnostic biomarkers. Simultaneously, machine learning is recognized as a significant complementary method for minimizing the resources needed for necessary measurement. Therefore, we applied two machine-learning algorithms, Lasso Cox regression analysis and random forest analysis, and the intersection of genes identified by these two algorithms was also performed. Fortunately, we ultimately screened out a gene, namely, *WIPF3* (Wiskott–Aldrich Syndrome Protein Family Member 3). WIPF3 (also known as CR16) belongs

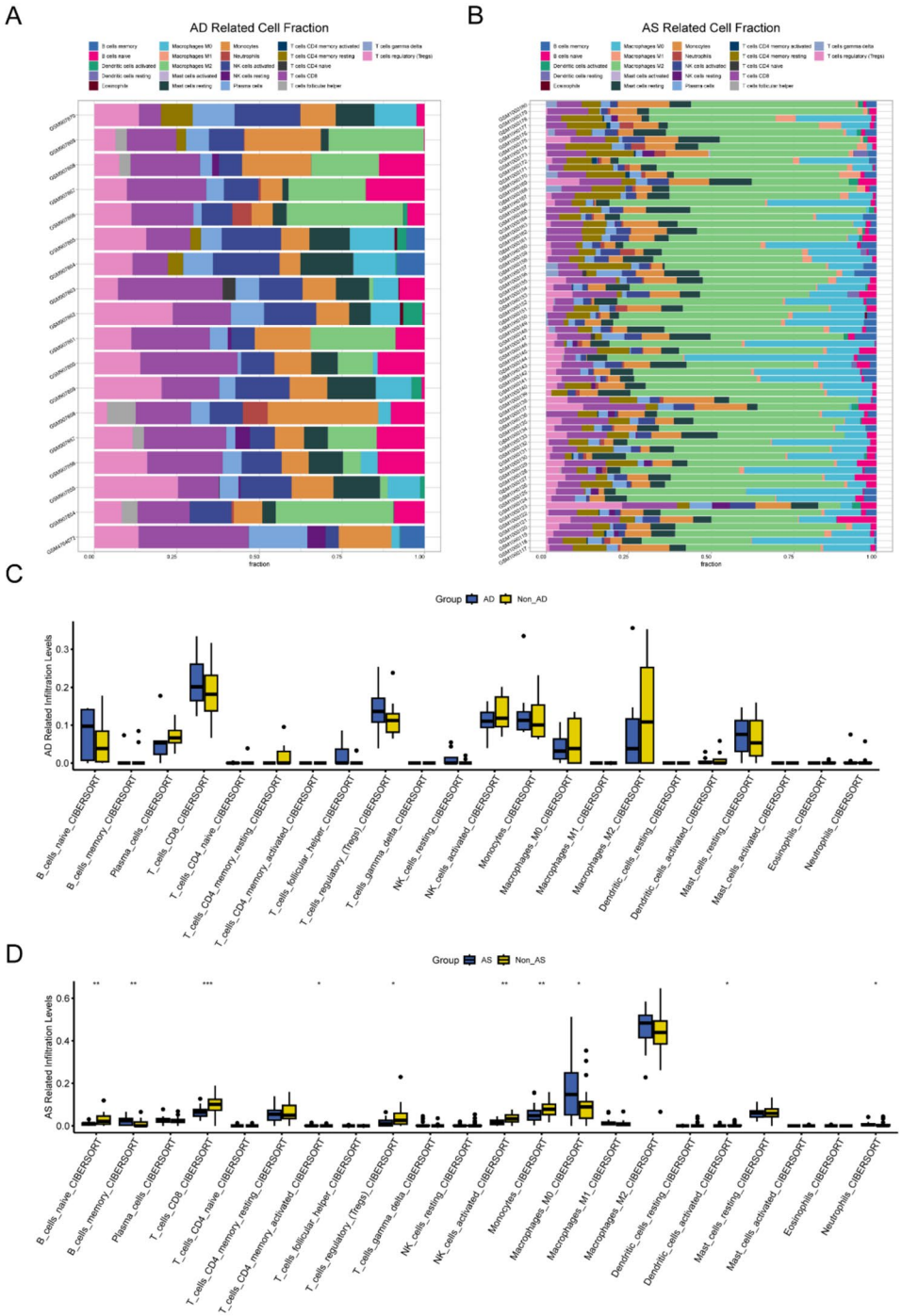

Fig. 7 Infiltration differences in 22 types of immune cells between diseased and normal samples in AD and AS. **A** Infiltration portion of 22 immune cell types in samples from AD and non-AD samples. **B** Infiltration portion of 22 immune cell types in samples from AS and non-AS samples. **C** Infiltration differences in 22 types of immune cells between AD and non-AD samples. **D** Infiltration differences in 22 types of immune cells between AS and non-AS samples

to the verprolin family, an actin-binding protein family. CR16 can express in brain and serve as a substrate for MAP kinase [28]. This study suggests that WIPF3 plays a potential role in mediating signaling pathways in the brain. In addition, in the bovine brain, CR16 is also found tightly associated with native N-WASP in a complex [29].

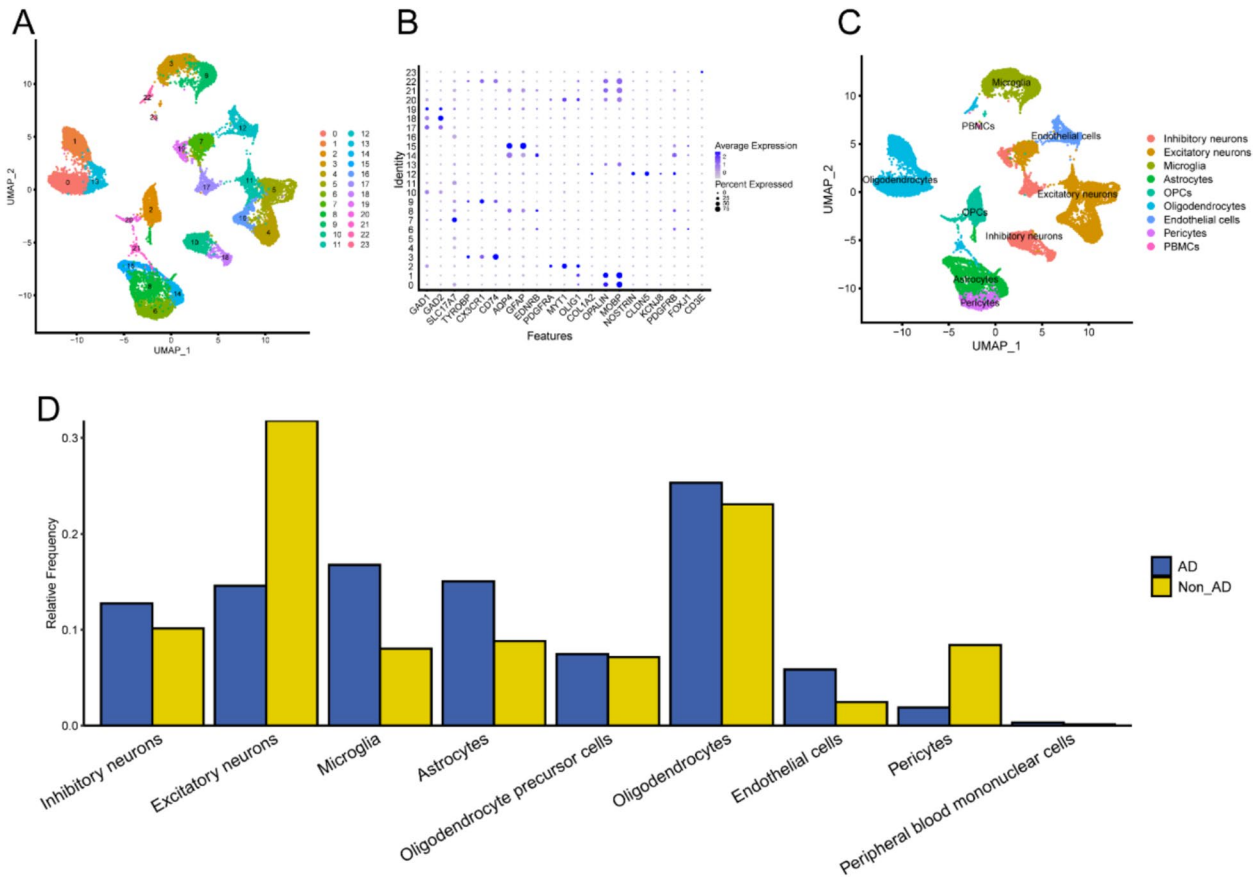

Fig. 8 Cell portion in 9 types of brain cells between AD and non-AD samples. **A** UMAP plot of cells from GSE175814, color-coded by cluster ID. **B** Dot plot expression of cell markers in 23 clusters. **C** UMAP plot of cells from GSE175814, color-coded by cell types. **D** Portion of cells from AD and non-AD samples in GSE175814

The N-WASP/WIPF3 complexes can trigger the activation of the Arp2/3 complex, leading to actin polymerization [29]. Dysfunctions in actin-binding proteins and impairments in actin polymerization increased the risk of AS [30–34]. Moreover, a postmortem study of abdominal aortic aneurysm reported that a non-synonymous variant in the *WIPF3* gene was involved in the aortic disorders [35]. These studies suggest that WIPF3 is vital in vascular functions. As Aβ might be the mediator of vascular dysfunction in AD [36], to further confirm the role of WIPF3 in AD and AS, we applied Aβ to treat the mouse vascular smooth muscle cell line MOVAS-1. The decrease of *WIPF3* levels in Aβ-treated MOVAS-1 cells indicated that WIPF3 is vital in the shared mechanism of AD and AS. In conclusion, these results strongly suggest that WIPF3 may play crucial roles in the pathogenesis of both AD and AS, and may serve as a potential mediator or mechanistic bridge in commonality between AD and AS. Moreover, enrichment analysis of key genes in AD and AS also revealed their relationship with the changes in vascular functions. It has been well-documented that the risk factors of vascular diseases also increase the incidence of AD, and cerebral amyloid angiopathy is of high prevalence in AD [37, 38]. These findings suggest that vascular dysfunction is vital in mediating the common pathogenesis of AD and AS.

WIPF3 is a promising target for understanding the pathogenesis of Alzheimer's disease (AD) and atherosclerosis (AS). Its role in these diseases may involve several key mechanisms, including cytoskeletal dynamics, immune regulation, and intercellular interactions. In AD, WIPF3 may influence disease progression by modulating cytoskeletal dynamics and immune responses. Studies have shown that WIPF3 expression remains stable in glomerular diseases but can change under certain pathological conditions [39]. This suggests that WIPF3 plays a crucial role in maintaining cell structure and function. In addition, the interaction between neurons and glial cells is critical in AD's pathological process [40], and WIPF3 may affect the signaling and function of these cells, contributing to the disease's progression. In AS, WIPF3's role is significant in the dynamic changes of the cytoskeleton

and the regulation of immune responses, which are crucial factors in disease progression. AS involves multiple factors, including lipid metabolism disorders, production of oxygen free radicals, and infiltration of inflammatory cells [41]. WIPF3 may exert its effects by influencing certain aspects of these processes, such as modulating cell motility and inflammatory responses. Furthermore, AS's pathological mechanisms also include endothelial cell dysfunction, smooth muscle cell proliferation, and migration [42]. WIPF3 may participate in the development and progression of AS by influencing the behavior of these cells. Studies have shown that AS is closely related to the expression and regulation of various inflammatory factors [43], and WIPF3 may play a role in regulating these factors. In summary, WIPF3's involvement in AD and AS may encompass multiple aspects, such as cytoskeletal dynamics, immune regulation, and intercellular interactions. Future research should focus on exploring the specific mechanisms of WIPF3 in these diseases to provide new ideas and strategies for treating related conditions.

Extensive research has consistently shown a strong connection between immune responses and the development of AD and AS [44–46]. They further suggest that the immune system holds promise as both a potential diagnostic indicator and a therapeutic target in managing AD and AS. Our WGCNA and subsequent GO and KEGG analysis also showed that both AD and AS key genes were related to immune responses. We proceeded to conduct immune cell infiltration analysis on both AD and AS data sets. The analysis revealed a significant difference in AS, but not in AD. The result showed that both the innate immune system and adaptive immune system were activated in AS. Consistent with previously reported, AS is classified as a chronic inflammatory vascular condition, and involves both innate and adaptive immune responses [47]. Anti-inflammatory interventions alongside the statin therapy yielded greater benefits compared to other adjunctive therapies in AS [48]. However, none of these cells were found to change in AD samples. This may be attributed to fact that the 22 immune cell types analyzed in immune cell infiltration analysis applies are predominantly abundant in the peripheral immune system. In the central nervous system, they may be undetectable by current methods due to their low abundances. Neuroinflammation has been considered important in AD for long. In addition, glial cells are considered to be the inflammatory cells in the central nervous system [49–51]. Hence, we conducted an analysis to assess the proportion of glial cells in AD based on single-cell RNA sequencing data. It revealed an increased portion of microglia and astrocytes in AD. Increased number or proliferation of microglia and astrocytes may suggest the occurrence of neuroinflammation in AD. These results confirm that inflammation plays a significant role in both AD and AS. However, the association between the inflammation in AD and in AS, even in the peripheral system and in central nervous system, still requires further investigation. Altogether, research focusing on the immune responses and mechanisms underlying the vascular dysfunction is worth considering.

Taken together, our analysis of shared mechanisms in AD and AS based on several bioinformatic methods has revealed two potential associations between AD and AS. Coupling WGCNA with machine learning-based Lasso Cox regression and random forest analysis has uncovered that WIPF3 has the potential to mediate the commonality between AD and AS. In addition, enrichment analysis and immune cell infiltration analysis have revealed the significance of inflammation in both AD and AS.

However, like many bioinformatics studies, our work also has several limitations. First, we acknowledge the challenges associated with integrating data from different disease models. Different disease models may have inherent differences in biological characteristics, experimental conditions, and sample sources, which may introduce biases and affect the accuracy and generalizability of our results. Second, our initial approach involved analyzing AD and AS separately and identifying overlapping mechanisms post hoc, rather than modeling them together in a unified framework. A more integrated modeling approach could provide a deeper understanding of shared pathophysiological processes. By separating the analyses, we may have overlooked some subtle but important interactions between the two diseases that could only be captured in a unified model. Third, the data sets of AD and AS come from different human tissues. While we have made efforts to analyze the data from each data set independently, the influence of tissue specificity on gene expression cannot be ignored. Gene expression patterns can vary significantly between different tissues, and this tissue-specific variability may mask or exaggerate the shared mechanisms we are trying to identify. Fourth, the experiments on the role of WIPF3 are relatively simple. More comprehensive experimental validations are needed to fully understand its role in the context of AD and AS. Although we have identified WIPF3 as a potential mediator, further investigation is required to determine its exact function, regulatory mechanisms, and interactions with other molecules.

Going forward, we can conduct biological experiments to confirm the specific role of WIPF3 or inflammation in the mechanisms of AD and AS. Furthermore, exploring the relationship between WIPF3 and inflammation may also provide new insights into the common mechanisms of AD and AS. These will facilitate the exploration of potential therapeutic targets that can be manipulated for

both AD and AS. We are also committed to addressing these limitations in future research to further improve our understanding of AD and AS and contribute to the development of more effective treatments.

Conclusions

This study provided a new perspective on understanding the shared mechanisms in AD and AS. Furthermore, we revealed a specific marker, WIPF3, has great potential to mediate the commonality between AD and AS.

Abbreviations

Aβ	Amyloid-β
AD	Alzheimer's disease
AS	Atherosclerosis
AUC	Area under the ROC curve
DEGs	Differentially expressed genes
GO	Gene Ontology
GSEA	Gene Set Enrichment Analysis
KEGG	Kyoto Encyclopedia of Genes Genomes
NK cells	Natural killer cells
ROC	Receiver operating characteristic
Tfhs	T follicular helper cells
Tgd cells	Gamma delta T cells
Tregs	Regulatory T cells
UMAP	Uniform Manifold Approximation and Projection
vSMC	Vascular smooth muscle cell
WGCNA	Weighted Gene Co-expression Network Analysis
SMC	Smooth muscle cell

Supplementary Information

The online version contains supplementary material available at https://doi.org/10.1186/s40001-025-02642-z.

Supplementary material 1. Supplement Fig. 1. The GO and KEGG analyses of gene modules identified by WGCNA in AD. A. The GO and KEGG analyses of the darkturquoise module genes. B. The GO and KEGG analyses of the brown4 module genes. Supplement Fig. 2. The GO and KEGG analyses of gene modules identified by WGCNA in AS. A. The GO and KEGG analyses of the black module genes. B. The GO and KEGG analyses of the brown module genes.

Acknowledgements

This work was supported by the grant from National Natural Science Foundation Project.

Author contributions

J.Y., J.W., and Z.W. conceived and designed the study. J.Y., and J.W. performed experiments and data analyses. J.Y., and Z.W. wrote the manuscript. All authors read and approved the final manuscript.

Funding

Not applicable.

Availability of data and materials

No datasets were generated or analysed during the current study.

Declarations

Ethics approval and consent to participate

Not applicable.

Consent for publication

All authors gave their consent for publication.

Competing interests

The authors declare no competing interests.

Received: 8 November 2024 Accepted: 27 April 2025
Published online: 22 May 2025

References

1. Cortes-Canteli M, Iadecola C. Alzheimer's disease and vascular aging: JACC focus seminar. J Am Coll Cardiol. 2020;75(8):942–51.
2. Masters CL, Bateman R, Blennow K, Rowe CC, Sperling RA, Cummings JL. Alzheimer's disease. Nat Rev Dis Primers. 2015;1:15056.
3. Sweeney MD, Montagne A, Sagare AP, Nation DA, Schneider LS, Chui HC, et al. Vascular dysfunction-the disregarded partner of Alzheimer's disease. Alzheimers Dement. 2019;15(1):158–67.
4. Iadecola C. The neurovascular unit coming of age: a journey through neurovascular coupling in health and disease. Neuron. 2017;96(1):17–42.
5. Arvanitakis Z, Capuano AW, Leurgans SE, Bennett DA, Schneider JA. Relation of cerebral vessel disease to Alzheimer's disease dementia and cognitive function in elderly people: a cross-sectional study. Lancet Neurol. 2016;15(9):934–43.
6. Bangen KJ, Nation DA, Delano-Wood L, Weissberger GH, Hansen LA, Galasko DR, et al. Aggregate effects of vascular risk factors on cerebrovascular changes in autopsy-confirmed Alzheimer's disease. Alzheimers Dement. 2015;11(4):394–403.
7. Toledo JB, Arnold SE, Raible K, Brettschneider J, Xie SX, Grossman M, et al. Contribution of cerebrovascular disease in autopsy confirmed neurodegenerative disease cases in the National Alzheimer's Coordinating Centre. Brain. 2013;136(Pt 9):2697–706.
8. Hofman A, Ott A, Breteler MM, Bots ML, Slooter AJ, van Harskamp F, et al. Atherosclerosis, apolipoprotein E, and prevalence of dementia and Alzheimer's disease in the Rotterdam Study. Lancet. 1997;349(9046):151–4.
9. Mohanta SK, Peng L, Li Y, Lu S, Sun T, Carnevale L, et al. Neuroimmune cardiovascular interfaces control atherosclerosis. Nature. 2022;605(7908):152–9.
10. Libby P. The changing landscape of atherosclerosis. Nature. 2021;592(7855):524–33.
11. Sturlaugsdottir R, Aspelund T, Bjornsdottir G, Sigurdsson S, Thorsson B, Eiriksdottir G, et al. Prevalence and determinants of carotid plaque in the cross-sectional REFINE-Reykjavik study. BMJ Open. 2016;6(11): e012457.
12. Hosoki S, Hansra GK, Jayasena T, Poljak A, Mather KA, Catts VS, et al. Molecular biomarkers for vascular cognitive impairment and dementia. Nat Rev Neurol. 2023;19(12):737–53.
13. Sabayan B, Goudarzi R, Ji Y, Borhani-Haghighi A, Olson-Bullis BA, Murray AM, et al. Intracranial atherosclerosis disease associated with cognitive impairment and dementia: systematic review and meta-analysis. J Am Heart Assoc. 2023;12(22): e032506.
14. Hartman RJG, Owsiany K, Ma L, Koplev S, Hao K, Slenders L, et al. Sex-stratified gene regulatory networks reveal female key driver genes of atherosclerosis involved in smooth muscle cell phenotype switching. Circulation. 2021;143(7):713–26.
15. Tyrrell DJ, Goldstein DR. Ageing and atherosclerosis: vascular intrinsic and extrinsic factors and potential role of IL-6. Nat Rev Cardiol. 2021;18(1):58–68.
16. Vermunt L, Sikkes SAM, van den Hout A, Handels R, Bos I, van der Flier WM, et al. Duration of preclinical, prodromal, and dementia stages of Alzheimer's disease in relation to age, sex, and APOE genotype. Alzheimers Dement. 2019;15(7):888–98.
17. Vemuri P, Lesnick TG, Przybelski SA, Knopman DS, Lowe VJ, Graff-Radford J, et al. Age, vascular health, and Alzheimer disease biomarkers in an elderly sample. Ann Neurol. 2017;82(5):706–18.
18. Song Y, Stampfer MJ, Liu S. Meta-analysis: apolipoprotein E genotypes and risk for coronary heart disease. Ann Intern Med. 2004;141(2):137–47.

19. Corder EH, Saunders AM, Strittmatter WJ, Schmechel DE, Gaskell PC, Small GW, et al. Gene dose of apolipoprotein E type 4 allele and the risk of Alzheimer's disease in late onset families. Science. 1993;261(5123):921–3.
20. Soreq L, Bird H, Mohamed W, Hardy J. Single-cell RNA sequencing analysis of human Alzheimer's disease brain samples reveals neuronal and glial specific cells differential expression. PLoS ONE. 2023;18(2): e0277630.
21. Hao Y, Hao S, Andersen-Nissen E, Mauck WM 3rd, Zheng S, Butler A, et al. Integrated analysis of multimodal single-cell data. Cell. 2021;184(13):3573–87.
22. Ghojogh B, Crowley M, Karray F, Ghodsi A. Uniform manifold approximation and projection (UMAP). In: Elements of dimensionality reduction and manifold learning. Cham: Springer; 2023.
23. Fan J, Shi S, Qiu Y, Liu M, Shu Q. Analysis of signature genes and association with immune cells infiltration in pediatric septic shock. Front Immunol. 2022;13:1056750.
24. Zeng D, Ye Z, Shen R, Yu G, Wu J, Xiong Y, et al. IOBR: multi-omics immuno-oncology biological research to decode tumor microenvironment and signatures. Front Immunol. 2021;12: 687975.
25. Leszek J, Mikhaylenko EV, Belousov DM, Koutsouraki E, Szczechowiak K, Kobusiak-Prokopowicz M, et al. The links between cardiovascular diseases and Alzheimer's disease. Curr Neuropharmacol. 2021;19(2):152–69.
26. Santos CY, Snyder PJ, Wu WC, Zhang M, Echeverria A, Alber J. Pathophysiologic relationship between Alzheimer's disease, cerebrovascular disease, and cardiovascular risk: a review and synthesis. Alzheimers Dement. 2017;7:69–87.
27. Korte N, Nortley R, Attwell D. Cerebral blood flow decrease as an early pathological mechanism in Alzheimer's disease. Acta Neuropathol. 2020;140(6):793–810.
28. Weiler MC, Smith JL, Masters JN. CR16, a novel proline-rich protein expressed in rat brain neurons, binds to SH3 domains and is a MAP kinase substrate. J Mol Neurosci. 1996;7(3):203–15.
29. Ho HY, Rohatgi R, Ma L, Kirschner MW. CR16 forms a complex with N-WASP in brain and is a novel member of a conserved proline-rich actin-binding protein family. Proc Natl Acad Sci USA. 2001;98(20):11306–11.
30. Allen A, Gau D, Roy P. The role of profilin-1 in cardiovascular diseases. J Cell Sci. 2021. https://doi.org/10.1242/jcs.249060.
31. Hu YW, Guo FX, Xu YJ, Li P, Lu ZF, McVey DG, et al. Long noncoding RNA NEXN-AS1 mitigates atherosclerosis by regulating the actin-binding protein NEXN. J Clin Invest. 2019;129(3):1115–28.
32. Singh RK, Haka AS, Bhardwaj P, Zha X, Maxfield FR. Dynamic actin reorganization and Vav/Cdc42-dependent actin polymerization promote macrophage aggregated LDL (low-density lipoprotein) uptake and catabolism. Arterioscler Thromb Vasc Biol. 2019;39(2):137–49.
33. Reschen ME, Lin D, Chalisey A, Soilleux EJ, O'Callaghan CA. Genetic and environmental risk factors for atherosclerosis regulate transcription of phosphatase and actin regulating gene PHACTR1. Atherosclerosis. 2016;250:95–105.
34. Hien TT, Turczynska KM, Dahan D, Ekman M, Grossi M, Sjogren J, et al. Elevated glucose levels promote contractile and cytoskeletal gene expression in vascular smooth muscle via rho/protein kinase c and actin polymerization. J Biol Chem. 2016;291(7):3552–68.
35. Maeda Y, Sato N, Naka-Mieno M, Mori S, Arai T, Tanaka M, et al. Association of non-synonymous variants in WIPF3 and LIPA genes with abdominal aortic aneurysm: an autopsy study. J Geriatr Cardiol. 2016;13(12):960–7.
36. Nortley R, Korte N, Izquierdo P, Hirunpattarasilp C, Mishra A, Jaunmuktane Z, et al. Amyloid beta oligomers constrict human capillaries in Alzheimer's disease via signaling to pericytes. Science. 2019. https://doi.org/10.1126/science.aav9518.
37. Ringman JM, Sachs MC, Zhou Y, Monsell SE, Saver JL, Vinters HV. Clinical predictors of severe cerebral amyloid angiopathy and influence of APOE genotype in persons with pathologically verified Alzheimer disease. JAMA Neurol. 2014;71(7):878–83.
38. Vasilevko V, Passos GF, Quiring D, Head E, Kim RC, Fisher M, et al. Aging and cerebrovascular dysfunction: contribution of hypertension, cerebral amyloid angiopathy, and immunotherapy. Ann N Y Acad Sci. 2010;1207:58–70.
39. De Luca F, Kha M, Swärd K, Johansson ME. Identification of ARMH4 and WIPF3 as human podocyte proteins with potential roles in immunomodulation and cytoskeletal dynamics. PLoS ONE. 2023;18(1): e0280270.
40. Bandyopadhyay S. Role of neuron and glia in Alzheimer's disease and associated vascular dysfunction. Front Aging Neurosci. 2021;13: 653334.
41. Zeng T, Lei G-L, Yu M-L, Zhang T-Y, Wang Z-B, Wang S-Z. The role and mechanism of various trace elements in atherosclerosis. Int Immunopharmacol. 2024;142(Pt B): 113188.
42. Kiełbowski K, Bakinowska E, Pawlik A. The potential role of connexins in the pathogenesis of atherosclerosis. Int J Mol Sci. 2023;24(3):2600.
43. Tang B-Y, Ge J, Wu Y, Wen J, Tang X-H. The role of ADAM17 in inflammation-related atherosclerosis. J Cardiovasc Transl Res. 2022;15(6):1283–96.
44. 2023 Alzheimer's disease facts and figures. Alzheimers Dement. 2023;19(4):1598-695
45. Stahr N, Galkina EV. Immune response at the crossroads of atherosclerosis and Alzheimer's disease. Front Cardiovasc Med. 2022;9: 870144.
46. Engelen SE, Robinson AJB, Zurke YX, Monaco C. Therapeutic strategies targeting inflammation and immunity in atherosclerosis: how to proceed? Nat Rev Cardiol. 2022;19(8):522–42.
47. Kong P, Cui ZY, Huang XF, Zhang DD, Guo RJ, Han M. Inflammation and atherosclerosis: signaling pathways and therapeutic intervention. Signal Transduct Target Ther. 2022;7(1):131.
48. Ridker PM. The time to initiate anti-inflammatory therapy for patients with chronic coronary atherosclerosis has arrived. Circulation. 2023;148(14):1071–3.
49. Gulen MF, Samson N, Keller A, Schwabenland M, Liu C, Gluck S, et al. cGAS-STING drives ageing-related inflammation and neurodegeneration. Nature. 2023;620(7973):374–80.
50. Moonen S, Koper MJ, Van Schoor E, Schaeverbeke JM, Vandenberghe R, von Arnim CAF, et al. Pyroptosis in Alzheimer's disease: cell type-specific activation in microglia, astrocytes and neurons. Acta Neuropathol. 2023;145(2):175–95.
51. Yang QQ, Zhou JW. Neuroinflammation in the central nervous system: symphony of glial cells. Glia. 2019;67(6):1017–35.

Publisher's Note